Journal of the Brazilian Society of Mechanical Sciences and Engineering (2018) 40:415
https://doi.org/10.1007/s40430-018-1330-2

REVIEW

Spectral element-based method for a one-dimensional damaged structure with distributed random properties

M. R. Machado[1] · S. Adhikari[2] · J. M. C. Dos Santos[3]

Received: 29 January 2018 / Accepted: 28 July 2018 / Published online: 9 August 2018

Abstract
Stochastic methods have received considerable attention because they address the randomness present in structural numerical models. Uncertainties represent important events in dynamic systems regarding vibration response prediction, especially in the mid- and high-frequency ranges, when responses have higher dispersions. The spectral element method (SEM) is suitable for analysing wave propagation problems based on large frequency ranges. It is a powerful tool for structural health monitoring. This paper unifies these two techniques to use the SEM with distributed randomness in the system parameters to model structural damage. Parameters are assumed to be distributed along the structure and expressed as a random field, which are expanded in the Karhunen–Loève spectral decomposition and memoryless transformation. A frequency-dependent stochastic stiffness and mass element matrices are formulated for bending vibration. Closed-form expressions are derived by the Karhunen–Loève expansion. Numerical examples are used to address the proposed methodology.

Keywords Spectral element method · Uncertainty quantification · Karhunen–Loève expansion · Memoryless transformation

1 Introduction

An effective and well-known technique used in many engineering areas is the finite element method (FEM) [1], a stochastic treatment [2–4]. Nevertheless, wave propagation-based models and high-frequency band analyses require many finite elements to obtain an accurate solution. In these cases, FEM solution can be expensive or infeasible from a computational perspective. An alternative is to use other suitable approaches, such as the spectral element method (SEM). With this method, the dynamic system governing equations written in the frequency domain is formulated using the concept of dynamic stiffness method (DSM) [5]. SEM is a meshing method similar to FEM, where the approximated element shape functions are substituted by shape functions obtained from the exact solutions to the governing differential equations. Therefore, a single element is enough to model any continuous and uniform part of the structure. This feature significantly reduces the number of elements required in the structure model and improves the accuracy of the dynamic system solution. In SEM, the responses are assumed to be wave-mode superposition procedures from the discrete Fourier transform (DFT) theory. Like FEM, mesh refinement can be applied to any discontinuity (e.g., geometric, material, external forces) in the spatial domain and assembly technique to form the global matrix equation. A linear problem solution is solved by using a matrix equation related to the global spectral nodal degrees-of-freedom (DoF). The inverse-DFT is used in cases of time domain solutions.

Because the SEM assumes an exact frequency domain solution, it implies high accuracy. Other advantages of this method are the reduction of the problem size and DOFs, low computational costs, effectiveness in dealing with frequency domain problems and adequate care with the non-reflecting boundary conditions of the infinite or semi-infinite domain problems [6]. There are some drawbacks,

Technical Editor: Marcelo A. Trindade.

✉ M. R. Machado
marcelam@unb.br

[1] Department of Mechanical Engineering, University of Brasília, Brasília 70910-900, Brazil

[2] Zienkiewicz Centre for Computational Engineering, Swansea University, Bay Campus, Swansea SA18EN, UK

[3] Department of Computational Mechanics, University of Campinas, Campinas, SP 13083-970, Brazil

however, such as the unavailability of exact wave solutions for more complex, 2-dimensional and 3-dimensional structures. However, approximated SEM can be used and may still provide an accurate solution. Whereas SEM ensures an exact frequency domain, it is not right for time domain solutions, because errors of aliasing or leakage, which are inevitable in the use of the inverse-DFT process, require particular attention. To avoid distortion caused by reflections, a damped structure or a semi-infinite (throw-off) element should be employed with a large time window [7].

In 1978, the first SEM proposal was presented by Beskos and Narayanan [8], called 'dynamic stiffness influence coefficients in flexural forced vibration.' They formulated the dynamic stiffness matrix for two uniform Euler–Bernoulli beam element nodes in a frequency domain using DFT theory. Their work was further improved and generalised by Spyrakso and Beskos [9]. SEM [6, 10] has different names, such as DSM [11–21], spectral FEM [22, 23] and dynamic FEM [24, 25]. Doyle [26] published his first work about SEM for longitudinal wave propagation in rods. He was the first to call this approach 'spectral element method.' Later, he presents an excellent compilation of works and other studies up to 1997 [7]. The book's content refers to SEM fundamentals with applications, mostly for wave propagations in structures. In 2004, another book about SEM was published by Lee [6], presenting an extensive study of the fundamentals and a variety of new applications (e.g., rotor dynamics, composite laminated, periodic lattice, damage detection) not covered by Doyle's book. A third book of SEM was published by Gopalakrishnan et al. [23], which was more focused on the wave behaviour of composites, inhomogeneous media and active vibration controls. More recently, a book with applications to structural health monitoring was published by Ostachowicz et al. [27].

Probabilistic treatment of uncertainties using SEM is a recent phenomenon. Works in this sense include papers by Ajith and Gopalakrishnan [28] and Adhikari [29]. Owing to SEM formulated with an exact wave propagation solution, it becomes a suitable technique to model damaged structures. Generally, changes in global or local structural properties can be associated with imperfections or damage. Over the last two decades, many vibration-based works have been developed for non-destructive evaluation tests and structural health monitoring. They use changes in modal parameters or dynamic responses to localise and quantify damage [30, 31]. These techniques are well suited to detect relatively large damages (i.e., not small), such as a crack. A structural crack does not impose significant changes in the low-frequency band, nor does it influence global structural behaviour. However, the presence of a crack in the structure introduces a local flexibility change that affects the vibrational response. It generates an evident change in the elastic waves that propagate through the structure. Consequently, in the last decades, damage detection researchers have focused on methods that use elastic wave propagations at medium- and high-frequency bands [32–36]. They use inherent material properties with discontinuities (e.g., cracks) to generate changes in the elastic waves propagating in the structure. There are some advantages to elastic wave-based damage detection, such as the capacity to propagate over significant distances and high sensitivities to discontinuities near the wave propagation path. Studies related to structural damage detection, including a stochastic treatment and wave propagation approaches, were also developed. Fabro et al. [37] presented a cracked rod modelled by SEM with randomness in the crack local flexibility. Ng et al. [38] in 2011 published a paper using a SEM-damaged rod structure and the Bayesian inference approach to determine the uncertain parameters. Machado et al. [39] proposed the damaged rod spectral element in a stochastic context. Other works that use wave propagation and SEM to detect damage in the presence of structural randomness can also be found in [40, 41].

The central goal of this paper is to develop a formulation for a stochastic approach of the SEM for a damaged one-dimensional (1D) structure. Thus, a new formulation for a damaged beam spectral element in a stochastic framework is presented. The random parameters are assumed to be spatially distributed and expressed by a random field. Considering that the mechanical system random field (e.g., stiffness and mass) should not be understood as a Gaussian distribution [42], the spectral decomposition known as the Karhunen–Loève (KL) expansion is applied for a non-Gaussian random field by using the memoryless transformation. Numerical simulations are used to demonstrate the proposed formulation.

2 Stochastic SEM

This section presents a review of the general derivation for the stochastic SEM [29] applied to dynamic mechanical systems and the non-Gaussian random parameters approximated by KL expansion.

2.1 General formulation

$(\Theta, \mathcal{F}, P)$ is a probability space, and $\theta \in \Theta$ denotes a sampling point in the sampling space, Θ. $\mathcal{F}$ is the complete σ-algebra over the subsets of Θ, and P is the probability measure. A linear damped distributed parameter dynamic system is governed by a linear partial differential equation [43] given by

$$\rho(\mathbf{r},t)\frac{\partial^2 U(\mathbf{r},t)}{\partial t^2}+\mathrm{L}_{10}(\theta)\frac{\partial U(\mathbf{r},t)}{\partial t}+\mathrm{L}_{20}(\theta)U(\mathbf{r},t) = q(\mathbf{r},t),\quad \mathbf{r}\in\mathcal{D},\quad t\in T, \tag{1}$$

where $U(\mathbf{r},t)$ is the displacement variable, $\rho(\mathbf{r},t)$ is the random mass distribution, $q(\mathbf{r},t)$ is the distributed time-varying forcing function, L_{10} is the random spatial self-adjoint damping operator, L_{20} is the random spatial self-adjoint stiffness operator, $\mathbf{r}\in\mathbb{R}^d$ is the spatial position vector, $d\leq 3$ is the dimension of the model specified in some domain, and $\mathcal{D}$ and t denote time domain. When parametric uncertainties are considered, the mass density, $\rho(\mathbf{r},t):(\mathbb{R}^d\times\Theta)\rightarrow\mathbb{R}$, and the stiffness operator involve a random process. The homogeneous deterministic system of Eq. (1), without any external force [43], is given by,

$$\rho_0\frac{\partial^2 U(\mathbf{r},t)}{\partial t^2}+L_{10}\frac{\partial U(\mathbf{r},t)}{\partial t}+L_{20}U(\mathbf{r},t)=0,\quad \mathbf{r}\in\mathcal{D}, \tag{2}$$

with a proper homogeneous boundary and initial conditions. Taking the Fourier transform of Eq. (2) and considering zero initial conditions, one obtains

$$-\omega^2\rho_0 u(\mathbf{r},\omega)+i\omega L_{10}\{u(\mathbf{r},\omega)\}+L_{20}\{u(\mathbf{r},\omega)\}=0, \tag{3}$$

where $\omega\in[0;\Omega]$ is the circular frequency and $\Omega\in\mathbb{R}$ is the maximum frequency. Like FEM, SEM considers that frequency-dependent displacement within an element is interpolated by using the nodal displacements as

$$u_e(\mathbf{r},\omega)=\mathbf{g}(\mathbf{r},\omega)\mathbf{d}(\omega), \tag{4}$$

where $\mathbf{d}(\omega)\in\mathbb{C}^n$ is the nodal displacement vector, $\mathbf{g}(\mathbf{r},\omega)\in\mathbb{C}^n$ is the vector of frequency-dependent shape functions, and n is number of the nodal DoF. Suppose the $s_j\in\mathbb{C}$, $j=1,2,\ldots,m$ are the basis functions that exactly satisfy Eq. (3), where m is the order of the ordinary differential equation. The shape function vector can then be expressed as

$$\mathbf{g}(\mathbf{r},\omega)=\mathbf{s}(\mathbf{r},\omega)\mathbf{\Gamma}(\omega), \tag{5}$$

where the vector, $\mathbf{s}(\mathbf{r},\omega)=\{s_j(\mathbf{r},\omega)\}^{\mathrm{T}};\ \forall j=1,2,\ldots,m$; and the complex matrix, $\mathbf{\Gamma}(\omega)\in\mathbb{C}^{n\times m}$, depends on the boundary conditions. The derivation of $\mathbf{\Gamma}(\omega)$ for the bending vibration of beams is given in the next sections.

By extending the weak-form of the finite element approach to a complex domain, the frequency-dependent $n\times n$ complex random stiffness and mass element matrices can be obtained as

$$\mathbf{K}(\omega,\theta)=\int_{\mathcal{D}}k_s(\mathbf{r},\theta)\mathcal{L}_2\{\mathbf{g}^{\mathrm{T}}(\mathbf{r},\omega)\}\mathcal{L}_2\{\mathbf{g}(\mathbf{r},\omega)\}\mathrm{d}\mathbf{r}. \tag{6}$$

$$\mathbf{M}(\omega,\theta)=\int_{\mathcal{D}}\rho(\mathbf{r},\theta)\mathbf{g}^{\mathrm{T}}(\mathbf{r},\omega)\mathbf{g}(\mathbf{r},\omega)\mathrm{d}\mathbf{r}, \tag{7}$$

where $(\bullet)^{\mathrm{T}}$ is the transpose matrix, $k_s(\mathbf{r},\theta):(\mathbb{R}^d\times\Theta)\rightarrow\mathbb{R}$ is the random distributed stiffness parameter, and $\mathcal{L}_2\{\bullet\}$ is the strain energy operator.

The uncertainty parameters are modelled within the framework of a random field and are treated similarly to the stochastic FEM proposed by Ghanem and Spanos [2]. The random fields, $k_s(\mathbf{r},\theta)$ and $\rho(\mathbf{r},\theta)$, are expanded using the KL expansion with a finite number of terms. Each complex element matrix can be expanded in a spectral series. For the case of the stiffness element matrix, it can be obtained as

$$\mathbf{K}(\omega,\theta)=\mathbf{K}_0(\omega)+\sum_{j=1}^{N_K}\xi_{Kj}(\theta)\mathbf{K}_j(\omega), \tag{8}$$

where N_K is the number of terms kept in the KL expansion and $\xi_{Kj}(\theta)$ are uncorrelated random variables. The complex deterministic symmetric stiffness element matrix is

$$\begin{aligned}\mathbf{K}_0(\omega)&=\int_{\mathcal{D}}k_{s_0}(\mathbf{r},\theta)\mathcal{L}_2\{\mathbf{g}^{\mathrm{T}}(\mathbf{r},\omega)\}\mathcal{L}_2\{\mathbf{g}(\mathbf{r},\omega)\}\mathrm{d}\mathbf{r}\\&=\mathbf{\Gamma}^{\mathrm{T}}(\omega)\left(\int_{\mathcal{D}}k_s(\mathbf{r},\theta)\mathcal{L}_2\{\mathbf{s}^{\mathrm{T}}(\mathbf{r},\omega)\}\mathcal{L}_2\{\mathbf{s}(\mathbf{r},\omega)\}\mathrm{d}\mathbf{r}\right)\mathbf{\Gamma}(\omega),\end{aligned} \tag{9}$$

and

$$\begin{aligned}\mathbf{K}_j(\omega)&=\sqrt{\lambda_{K_j}}\int_{\mathcal{D}}\varphi_{K_j}(\mathbf{r})\mathcal{L}_2\{\mathbf{g}^{\mathrm{T}}(\mathbf{r},\omega)\}\mathcal{L}_2\{\mathbf{g}(\mathbf{r},\omega)\}\mathrm{d}\mathbf{r}\\&=\sqrt{\lambda_{K_j}}\,\mathbf{\Gamma}^{\mathrm{T}}(\omega)\left(\int_{\mathcal{D}}\varphi_{K_j}(\mathbf{r})\mathcal{L}_2\{\mathbf{s}^{\mathrm{T}}(\mathbf{r},\omega)\}\mathcal{L}_2\{\mathbf{s}(\mathbf{r},\omega)\}\mathrm{d}\mathbf{r}\right)\mathbf{\Gamma}(\omega)\\&\quad\forall j=1,2,\ldots,M_K,\end{aligned} \tag{10}$$

where λ_{Kj} and φ_{Kj} are the eigenvalues and eigenfunctions satisfying the integral equation of covariance function (Eq. 14). Equivalent equations corresponding to the mass element matrix can be obtained similarly. The spectral dynamic stiffness element matrix, expressed as a function of the stiffness and mass element matrix, is

$$\mathbf{D}(\omega,\theta)=\mathbf{K}(\omega,\theta)-\omega^2\mathbf{M}(\omega,\theta), \tag{11}$$

where $\mathbf{D}(\omega,\theta)$ is a complex random symmetric element matrix that needs to be inverted for every ω to obtain the dynamic response. In the next sections, this approach is applied to the damaged beam model.

2.2 KL expansion

In probability theory, a stochastic or random process is indexed by a subset of the real random variables representing the evolution of some system of random values over time. It can also consider more general parameter

spaces so that the stochastic process becomes a random function of more than one variable. This type of stochastic process is usually called a random field [44]. Various points expressed by random variables describe a random field. Thus, many mathematical procedures can be used to solve the resulting discrete stochastic differential equations. The method applied here is a random field spectral decomposition using KL expansion. Therefore, many points are required for a good approximation. The nonzero mean random process is decomposed as follows.

$$\varpi(\mathbf{x},\theta) = \varpi_0(\mathbf{x}) + Y(\mathbf{x},\theta), \tag{12}$$

where $\varpi_0(\mathbf{x})$ implies the corresponding expected value and $Y(\mathbf{x},\theta)$ is a random field with the covariance function, $C(\mathbf{x}_1,\mathbf{x}_2)$ defined in a space, $\mathcal{D}$. By definition, $C(\mathbf{x}_1,\mathbf{x}_2)$ is finite, symmetric and positive definite. Then, the random field can be written as

$$Y(\mathbf{x},\theta) = \sum_{j=1}^{\infty} \xi_j(\theta)\sqrt{\lambda_j}\varphi_j(\mathbf{x}), \tag{13}$$

where $\xi_j(\theta)$ are uncorrelated random variables and λ_j and $\varphi_j(\mathbf{x})$ are, respectively, eigenvalues and eigenfunctions satisfying the Fredholm integral equation:

$$\int_{\mathcal{D}} C(\mathbf{x}_1,\mathbf{x}_2)\varphi_j(\mathbf{x}_1)\mathrm{d}\mathbf{x}_1 = \lambda_j\varphi_j(\mathbf{x}_2) \quad \forall j = 1,2,\ldots. \tag{14}$$

By multiplying Eq. (13) by $\varphi_j(\mathbf{x})$ and integrating over the domain, $\mathcal{D}$, an explicit expression for $\xi_j(\theta)$, is obtained as

$$\xi_j(\theta) = \frac{1}{\sqrt{\lambda_j}}\int_{\mathcal{D}} Y(\mathbf{x},\theta)\varphi_j(\mathbf{x})\mathrm{d}\mathbf{x}, \tag{15}$$

with mean and covariance functions given by

$$\begin{aligned} &\mathbb{E}[\xi_i(\theta)] = 0, \\ &\mathbb{E}[\xi_i(\theta)\xi_j(\theta)] = \delta_{ij}, \end{aligned} \tag{16}$$

where δ_{ij} is the Kronecker-delta function. The integral in Eq. (15) can be interpreted as an infinite series of zero mean uncorrelated random variables. If the process, $\varpi(\mathbf{x},\theta)$, has a Gaussian marginal probability density function (PDF), $Y(\mathbf{x},\theta)$, it reduces to a zero mean Gaussian variable for a fixed position, x [42]. The KL coefficients are independent uncorrelated standard Gaussian variables. By applying the expansion to real cases, the infinite series is truncated with N terms to obtain $\varpi(\mathbf{x},\theta)$. Rewriting Eq. (12), one has

$$\varpi(\mathbf{x},\theta) = \varpi_0(\mathbf{x}) + \sum_{j=1}^{N} \xi_j(\theta)\sqrt{\lambda_j}\varphi_j(\mathbf{x}). \tag{17}$$

The spectral decomposition of the covariance function implies the solution of Eq. (14). Some covariance functions can be solved analytically, such as the first-order Markov processes, given by

$$C(x_1,x_2) = e^{-|x_1-x_2|/\mathtt{b}}, \tag{18}$$

where $\mathtt{b}$ is the correlation length, an important parameter to describe the random field. A random field becomes a random variable when the correlation length is large, compared to the domain under consideration. An analytical solution in the interval $-\mathtt{a} < x < \mathtt{a}$, where it is assumed that the mean is zero, produces a random field for Eq. (17). Given $\mathtt{c} = 1/\mathtt{b}$, the corresponding eigenvalues and eigenfunctions for odd j are given by

$$\begin{aligned} &\lambda_j = \frac{2\mathtt{c}}{w_j^2 + \mathtt{c}^2}; \quad \varphi_j(r) = \frac{\cos(w_j\frac{L}{2})}{\sqrt{\mathtt{a} + \frac{\sin(2w_j\mathtt{a})}{2w_j}}} \\ &\text{where} \quad \tan(w_j\mathtt{a}) = \frac{\mathtt{c}}{w_j}, \end{aligned} \tag{19}$$

and for even j, expressed as

$$\begin{aligned} &\lambda_j = \frac{2\mathtt{c}}{w_j^2 + \mathtt{c}^2}; \quad \varphi_j(r) = \frac{\sin(w_j\frac{L}{2})}{\sqrt{\mathtt{a} - \frac{\sin(2w_j\mathtt{a})}{2w_j}}} \\ &\text{where} \quad \tan(w_j\mathtt{a}) = \frac{w_j}{-\mathtt{c}}. \end{aligned} \tag{20}$$

2.3 Non-Gaussian process using memoryless transformation

Owing to the simplicity and symmetry of the Gaussian distribution, it is often assumed random properties can be modelled in engineering analysis [45, 46]. However, some realistic processes and fields do not follow the Gaussian distribution. Some material properties, such as Young's modulus, are quantities that cannot take negative values, and some processes, such as wind velocity, follow distributions that are non-Gaussian [47]. Schevenels et al. [42] demonstrated analytically and numerically that the variance of the displacement of a mechanical system with a Gaussian stiffness subjected to a deterministic force is infinite. Thus, such a system is physically inconsistent, and a random stiffness should not be assumed to be Gaussian. Therefore, a KL-series expansion for a non-Gaussian stochastic field is used, employing a non-Gaussian process, expressed as a memoryless transformation of an underlying Gaussian process. The memoryless transformation is a nonlinear mapping from a specified probability distribution to a target or request distribution. This method allows starting with any distribution and converting it into a target one. Here, the application regards it a correlated Gaussian stochastic process and produces a correlated process having the distributional characteristics of interest. In more detail, the concept and implementation of memoryless transformation can be found in [42, 45, 48, 49].

The main idea of most techniques for simulating a non-Gaussian, scalar or random field, $R(t)$, with a prescribed correlation function, $C_R(\tau)$, and a prescribed 1D marginal cumulative density function (CDF), $F_R(x)$, is to generate a zero mean and unit variance, scalar or Gaussian random field, $Z(t)$, with a prefixed correlation function, $C_Z(\tau)$, and mapping (transformation), $Z(t) \longrightarrow R(t)$, according to

$$R(t) = g[Z(t)], \tag{21}$$

where $g[\bullet]$ is an adequate function. This procedure is called a *memoryless* transformation, because the value of $R(t)$ at an arbitrary t_1 depends only on the value of $Z(t_1)$ and not on any other past or future values of $Z(t)$.

In this paper, the following technique is applied. The covariance function, $C(\mathbf{x}_1, \mathbf{x}_2)$, of the underlying Gaussian process, is chosen so that the transformation leads to a non-Gaussian process with the prescribed covariance function, $C_R(\mathbf{x}_1, \mathbf{x}_2)$. A non-Gaussian process, $Y(\mathbf{x}, \theta)$, is expressed as a memoryless transformation of an underlying standard Gaussian process, $Z(\mathbf{x}, \theta)$, through the CDFs of both processes:

$$Y(\mathbf{x}, \theta) = F_{Y_x}^{-1}\{F_Z[Z(\mathbf{x}, \theta)]\}, \tag{22}$$

where $F_{Y_x}(y)$ is the marginal CDF of the non-Gaussian process, $F_Z(z)$ is the standard Gaussian CDF, and the function $g[\bullet] = F_{Y_x}^{-1}\{F_Z[\bullet]\}$.

In the case that an analytical solution is not feasible, it is necessary to apply numerical methods. An approximation of the transformation can be obtained regarding the 1D polynomial chaos of order P:

$$Y(\mathbf{x}, \theta) \approx \sum_{n=0}^{P} a_n(\mathbf{x}) \mathtt{h}_n(Z(\mathbf{x}, \theta)), \tag{23}$$

where $\mathtt{h}_n$ is the n-order 1D Hermite polynomial, given by

$$\mathtt{h}_n(z) = \frac{1}{\sqrt{n!}} \mathtt{H}_n(z). \tag{24}$$

The polynomial, $\mathtt{H}_n(z)$, follows from the recurrence relation,

$$\mathtt{H}_0(z) = 1 \qquad \mathtt{H}_1(z) = z \qquad \mathtt{H}_{n+1}(z) = z\mathtt{H}_n(z) - n\mathtt{H}_{n-1}(z). \tag{25}$$

Owing to the orthonormality of the Hermite polynomials concerning the Gaussian probability distribution, the coefficients are obtained as

$$a_n(\mathbf{x}) = \int_{\infty}^{\infty} F_{Yx}^{-1}(F_Z(z)) \mathtt{h}_n(z) p_Z(z) \mathrm{d}z, \tag{26}$$

where $p_Z(z)$ is the standard Gaussian PDF. The covariance function of the non-Gaussian process becomes

$$C_R(\mathbf{x}_1, \mathbf{x}_2) \approx \sum_{n=0}^{P} a_n(\mathbf{x}_1) a_n(\mathbf{x}_2) [C(\mathbf{x}_1, \mathbf{x}_2)]^n. \tag{27}$$

Considering $Y(\mathbf{x}, \theta)$ is a stationary process, the covariance can be reduced to

$$C_R(\Delta\mathbf{x}) \approx \sum_{n=0}^{P} a_n^2 [C(\Delta\mathbf{x})]^n. \tag{28}$$

The covariance function of the underlying Gaussian process is obtained by solving Eq. (28) for every distance, $\Delta\mathbf{x}$, to produce a nonnegative definite function, $C(\Delta\mathbf{x})$. Then KL decomposition of the underlying Gaussian process is performed (Sect. 2.2). Realisations of this process are generated and transformed into realisations of the non-Gaussian process, $Y(x, \theta)$, using Eq. (22).

The non-Gaussian realisations are projected on the KL modes (Eq. 15) to produce the realisations of the non-Gaussian KL coefficients required to solve the SEM equations.

The Monte Carlo method, used as a stochastic solver, consists of solving the problem repeated times, each using a new random input. The mean and the standard deviation of the result are calculated through the generated samples. Let $X(\xi, \omega)$ be the frequency response of the stochastic system calculated for a realisation, ξ, generated by the Monte Carlo method [50]. The mean-square convergence analysis concerning independent realisations of the random variable, X, denoted by $X_j(\xi, \omega)$, is accomplished by studying the function, $n_S \mapsto \mathrm{conv}(n_S)$, defined by:

$$\mathrm{conv}(n_S) = \frac{1}{n_S} \sum_{j=1}^{n_S} \int_B \left\| X_j(\xi, \omega) \right\|^2 \mathrm{d}\omega. \tag{29}$$

3 1D damaged structures by SEM

This section presents the regular deterministic and the proposed stochastic formulations for damaged beam SEMs, a complete formulation for a rod can be found in reference [39].

3.1 Deterministic beam model

A spectral damaged Euler–Bernoulli beam element with a transverse, open and non-propagating crack [32, 51] is addressed. Figure 1 shows a two-node damaged beam element with uniform rectangular cross section, length L, crack position L_1, and crack depth α. The crack is modelled by dimensionless local crack flexibility, Θ_b.

The undamped equilibrium equation in the frequency domain can be written as [6]

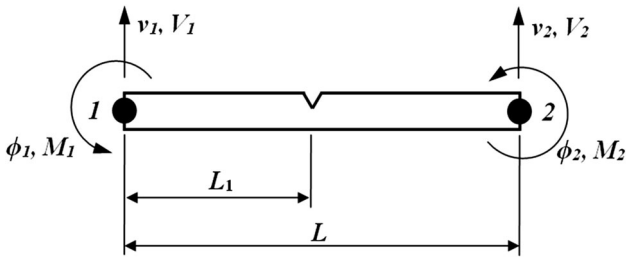

Fig. 1 Two-node damaged beam spectral element

$$EI\frac{\mathrm{d}^4 v(x)}{\mathrm{d}x^4} + \omega^2 \rho A v(x) = p(x), \tag{30}$$

where I is the inertia moment, v is the transverse displacement, and p is the distributed external transversal force. Structural internal damping is introduced into the beam formulation by adding a complex damping factor in the flexural rigidity, EI. In the deterministic case of $EI = EI_0(1 + i\eta)$, where EI_0 is the flexural rigidity deterministic value, η is the damping factor and i is the imaginary unit. In the stochastic case, it is given by $EI(\theta) = \hat{EI}(\theta) + EI_0 i\eta$, where the random part of flexural rigidity is a real value, $\hat{EI}(\theta)$, and the deterministic part is the complex value, $EI_0 i\eta$. The homogeneous displacement solution for Eq. (30) must be described in two parts, one for the left-hand side of the crack, $v_L(x)$, and another for the right-hand side of the crack, $v_R(x)$. From the general formulation (Sect. 2.1) one has

$$\begin{aligned} v_L(x) &= a_1 e^{-i(k_b x)} + a_2 e^{-(k_b x)} + a_3 e^{-ik_b(L_1 - x)} \\ &\quad + a_4 e^{-k_b(L_1 - x)} \quad (0 \le x \le L_1) \\ &= \mathbf{s}_L(x,\omega)\mathbf{a}_L, \end{aligned} \tag{31}$$

where $k_b = \sqrt{\omega}(\rho A/EI)^{1/4}$ is the beam wavenumber, $\mathbf{s}_L(x,\omega) = \left[e^{-i(k_b x)}\ e^{-(k_b x)}\ e^{-ik_b(L_1 - x)}\ e^{-k_b(L_1 - x)}\right]$, $\mathbf{a}_L = \{a_1\ a_2\ a_3\ a_4\}^{\mathrm{T}}$, and

$$\begin{aligned} v_R(x) &= a_5 e^{-ik_b(L_1 + x)} + a_6 e^{-k_b(L_1 + x)} + a_7 e^{-ik_b(L - (L_1 + x))} \\ &\quad + a_8 e^{-k_b(L - (L_1 + x))} \quad (0 \le x \le L - L_1) \\ &= \mathbf{s}_R(x,\omega)\mathbf{a}_R, \end{aligned} \tag{32}$$

where $\mathbf{s}_R(x,\omega) = \left[e^{-ik_b(L_1 + x)}\ e^{-k_b(L_1 + x)}\ e^{-ik_b(L - (L_1 + x))}\ e^{-k_b(L - (L_1 + x))}\right]$, and $\mathbf{a}_R = \{a_5\ a_6\ a_7\ a_8\}^{\mathrm{T}}$.

Writing Eqs. (31) and (32) in a matrix form,

$$\begin{Bmatrix} v_L(x) \\ v_R(x) \end{Bmatrix} = \mathbf{d} = \begin{bmatrix} \mathbf{s}_L(x,\omega) & \mathbf{0} \\ \mathbf{0} & \mathbf{s}_R(x,\omega) \end{bmatrix} \begin{Bmatrix} \mathbf{a}_L \\ \mathbf{a}_R \end{Bmatrix} = \mathbf{s}(x,\omega)\mathbf{a}, \tag{33}$$

where $\mathbf{d}$ is the nodal displacement vector, $\mathbf{a}$ is the coefficient vector, and $\mathbf{s}$ is a matrix dependent on the element boundary and compatibility conditions. The element boundary conditions are given by $v_L(0) = v_1$ and $\partial v_L(0)/\partial x = \phi_1$ at node 1 and $v_R(L - L_1) = v_2$ and $\partial v_R(L - L_1)/\partial x = \phi_2$ at node 2. Compatibility conditions are given by displacement at crack position, where $\partial v_L(L_1)/\partial x - \partial v_R(0)/\partial x = \Theta_b \partial^2 v_L(L_1)/\partial x^2$ at cracked region of the cross section and $v_L(L_1) = v_R(0)$, $\partial^2 v_L(L_1)/\partial x^2 = \partial^2 v_R(0)/\partial x^2$ and $\partial^3 v_L(L_1)/\partial x^3 = \partial^3 v_R(0)/\partial x^3$ at the non-cracked region of the cross section.

Applying boundary and compatibility conditions in Eq. (33) it has,

$$\underbrace{\begin{bmatrix} 1 & 1 & \mathsf{m} & \mathsf{n} & 0 & 0 & 0 & 0 \\ -ik & -k & ik\mathsf{m} & k\mathsf{n} & 0 & 0 & 0 & 0 \\ -\mathsf{m} & -\mathsf{n}- & -1 & -1 & \mathsf{m} & \mathsf{n} & \mathsf{o} & \mathsf{p} \\ i\mathsf{m}k - \mathsf{m}\Theta_b k^2 & \mathsf{n}k + \mathsf{n}\Theta_b k^2 & -ik - \Theta_b k^2 & -k + \Theta_b k^2 & -ik\mathsf{m} & -k\mathsf{n} & ik\mathsf{o} & k\mathsf{p} \\ -k^2\mathsf{m} & k^2\mathsf{n} & -k^2 & k^2 & k^2\mathsf{m} & -k^2\mathsf{n} & k^2\mathsf{o} & -k^2\mathsf{p} \\ ik^3\mathsf{m} & -k^3\mathsf{n} & -ik^3 & k^3 & -k^3\mathsf{m} & k^3\mathsf{n} & ik^3\mathsf{o} & -k^3\mathsf{p} \\ 0 & 0 & 0 & 0 & \mathsf{r} & \mathsf{t} & 1 & 1 \\ 0 & 0 & 0 & 0 & -ik\mathsf{r} & -k\mathsf{t} & ik & k \end{bmatrix}}_{\mathbf{G}_b} \begin{Bmatrix} a_1 \\ a_2 \\ a_3 \\ a_4 \\ a_5 \\ a_6 \\ a_7 \\ a_8 \end{Bmatrix} = \begin{Bmatrix} v_1 \\ \phi_1 \\ 0 \\ 0 \\ 0 \\ 0 \\ v_2 \\ \phi_2 \end{Bmatrix}, \tag{34}$$

where $\mathsf{m} = e^{ikL_1}$, $\mathsf{n} = e^{-kL_1}$, $\mathsf{o} = e^{-ik(L - L_1)}$, $\mathsf{p} = e^{k(L - L_1)}$, $\mathsf{r} = e^{-ikL}$ and $\mathsf{t} = e^{-kL}$. From Eq. (34), we can relate the coefficient vector with the nodal displacement vector by

$$\mathbf{a} = \mathbf{G}_{br}^{-1}\mathbf{d}, \tag{35}$$

where $\mathbf{G}_{br}^{-1}$ is the inverse of $\mathbf{G}_b$ reduced to the order $[8 \times 4]$, owing to the zeros in the displacement vector, $\mathbf{d}$. Substituting Eq. (3.1) into (33) one has,

$$\begin{Bmatrix} v_L(x) \\ v_R(x) \end{Bmatrix} = \begin{bmatrix} \mathbf{s}_L(x,\omega) & \mathbf{0} \\ \mathbf{0} & \mathbf{s}_R(x,\omega) \end{bmatrix} \mathbf{G}_{br}^{-1}\mathbf{d} = \mathbf{g}(x,\omega)\mathbf{d}, \tag{36}$$

where $\mathbf{g}(x,\omega)$ is the frequency-dependent shape function. Comparing Eq. (36) with (5), we learn that

$$\mathbf{\Gamma}(\omega) = \mathbf{G}_{br}^{-1}. \tag{37}$$

The stiffness operator is given by $\mathcal{L}_2(\bullet) = \partial^2(\bullet)/\partial x^2 = (\bullet)''$, and, assuming constant nominal values for the deterministic stiffness and mass parameter, $k_{s_0}(\mathbf{r}) = EI_0$ and $m_{s_0}(\mathbf{r}) = \rho A_0$, respectively. Because spatial reference in damaged model equations must be integrated according to the corresponding limits, then

$$\mathbf{K}_0(\omega) = EI_0\ \mathbf{\Gamma}_d^{\mathrm{T}}(\omega) \begin{bmatrix} \mathbf{Sk}_{0L} & \mathbf{0} \\ \mathbf{0} & \mathbf{Sk}_{0R} \end{bmatrix} \mathbf{\Gamma}(\omega), \tag{38}$$

$$\mathbf{M}_0(\omega) = \rho A_0\ \mathbf{\Gamma}_d^{\mathrm{T}}(\omega) \begin{bmatrix} \mathbf{Sm}_{0L} & \mathbf{0} \\ \mathbf{0} & \mathbf{Sm}_{0R} \end{bmatrix} \mathbf{\Gamma}(\omega), \tag{39}$$

where

$$\begin{aligned} \mathbf{Sk}_{0L} &= \int_0^{L_1} \mathbf{s}''^{\mathrm{T}}_L(x,\omega)\mathbf{s}''_L(x,\omega)\mathrm{d}x, \\ \mathbf{Sk}_{0R} &= \int_0^{(L-L_1)} \mathbf{s}''^{\mathrm{T}}_R(x,\omega)\mathbf{s}''_R(x,\omega)\mathrm{d}x, \end{aligned} \tag{40}$$

$$\begin{aligned} \mathbf{Sm}_{0L} &= \int_0^{L_1} \mathbf{s}^{\mathrm{T}}_L(x,\omega)\mathbf{s}_L(x,\omega)\mathrm{d}x, \\ \mathbf{Sm}_{0R} &= \int_0^{(L-L_1)} \mathbf{s}^{\mathrm{T}}_R(x,\omega)\mathbf{s}_R(x,\omega)\mathrm{d}x. \end{aligned} \tag{41}$$

Substituting Eq. (40) in Eq. (38) and Eq. (41) in Eq. (39), the deterministic stiffness and mass matrices as closed-form expressions can be obtained.

3.1.1 Bending crack flexibility

The bending crack flexibility can also be obtained from the Castigliano's theorem, considering that only crack mode I is shown in the beam element. Figure 2 can represent the damaged beam element cross section at the crack position, including the geometric definitions of crack depth as $\alpha = a/h$.

Crack flexibility coefficient can be written as a function of the crack depth by [32],

$$\mathtt{c}(\bar{\alpha}) = \frac{72\pi}{bh^2}\int_0^{\bar{a}} \bar{\alpha}\mathtt{f}^2(\bar{\alpha})\mathrm{d}\bar{a}, \tag{42}$$

where $\bar{a} = a/h$, $\bar{\alpha} = \alpha/h$, and

$$\mathtt{f}\left(\frac{\alpha}{h}\right) = \sqrt{\frac{2h}{\pi\alpha}\tan\left(\frac{\pi\alpha}{2h}\right)}\,\frac{0.923 + 0.199\left[1 - \sin\left(\frac{\pi\alpha}{2h}\right)\right]^4}{\cos\left(\frac{\pi\alpha}{2h}\right)}. \tag{43}$$

The dimensionless local crack-bending flexibility can be written as

$$\Theta_b = \frac{EI\mathtt{c}}{L}. \tag{44}$$

3.2 Stochastic beam model

The stochastic dynamic stiffness element matrix for the damaged beam spectral element, $\mathbf{D}_d(\omega,\theta)$, is developed. Flexural rigidity, EI, and mass per unit of length ρA are assumed distributed random fields, respectively, as

$$EI(x,\theta) = EI_0[1 + \varepsilon_1\varpi_1(x,\theta)], \tag{45}$$

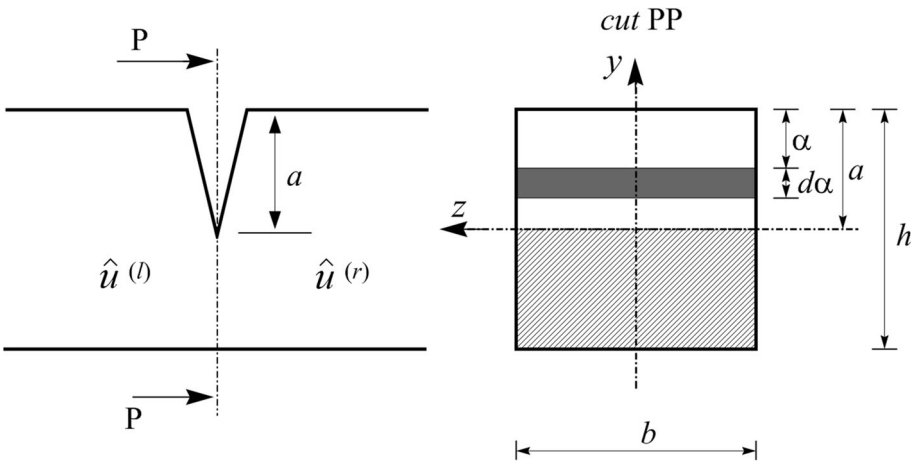

Fig. 2 Damaged structure cross section at the crack position

and

$$\rho A(x,\theta) = \rho A_0[1 + \varepsilon_2 \varpi_2(x,\theta)]. \tag{46}$$

Following Eq. (8), we can express the stochastic damaged beam stiffness and mass element matrices, respectively, as

$$\mathbf{K}_d(\omega,\theta) = \mathbf{K}_{0_d}(\omega) + \Delta\mathbf{K}_d(\omega,\theta), \tag{47}$$

$$\mathbf{M}_d(\omega,\theta) = \mathbf{M}_{0_d}(\omega) + \Delta\mathbf{M}_d(\omega,\theta). \tag{48}$$

From the KL expansion and Eqs. (45) and (46) one has,

$$\Delta\mathbf{K}_d(\omega,\theta) = \varepsilon_1 \sum_{j=1}^{N} \xi_{Kj}(\theta)\sqrt{\lambda_{Kj}}\mathbf{K}_{j_d}(\omega), \tag{49}$$

$$\Delta\mathbf{M}_d(\omega,\theta) = \varepsilon_2 \sum_{j=1}^{N} \xi_{Mj}(\theta)\sqrt{\lambda_{Mj}}\mathbf{M}_{j_d}(\omega). \tag{50}$$

where N is the number of terms kept in the KL expansion and $\xi_{Kj}(\theta)$ and $\xi_{Mj}(\theta)$ are uncorrelated Gaussian random variables with zero mean and unit standard deviation. From Eq. (10), and considering different limits of integration (left and right-hand sides) for the damaged beam model, one has

$$\mathbf{K}_{j_d}(\omega) = EI_0\boldsymbol{\Gamma}_d^{\mathrm{T}}(\omega)\begin{bmatrix}\mathbf{Sk}_L & \mathbf{0}\\ \mathbf{0} & \mathbf{Sk}_R\end{bmatrix}\boldsymbol{\Gamma}_d(\omega), \tag{51}$$

$$\mathbf{M}_{j_d}(\omega) = \rho A_0\boldsymbol{\Gamma}_d^{\mathrm{T}}(\omega)\begin{bmatrix}\mathbf{Sm}_L & \mathbf{0}\\ \mathbf{0} & \mathbf{Sm}_R\end{bmatrix}\boldsymbol{\Gamma}_d(\omega), \tag{52}$$

where

$$\begin{aligned}\mathbf{Sk}_L &= \int_0^{L_1} \varphi_{Kj}(x_e+x)\mathbf{s}''^{\mathrm{T}}_L(x,\omega)\mathbf{s}''_L(x,\omega)\mathrm{d}x,\\ \mathbf{Sk}_R &= \int_0^{(L-L_1)} \varphi_{Kj}(x_e+x)\mathbf{s}''^{\mathrm{T}}_R(x,\omega)\mathbf{s}''_R(x,\omega)\mathrm{d}x\end{aligned} \tag{53}$$

$$\begin{aligned}\mathbf{Sm}_L &= \int_0^{L_1} \varphi_{Mj}(x_e+x)\mathbf{s}_L^{\mathrm{T}}(x,\omega)\mathbf{s}_L(x,\omega)\mathrm{d}x,\\ \mathbf{Sm}_R &= \int_0^{(L-L_1)} \varphi_{Mj}(x_e+x)\mathbf{s}_R^{\mathrm{T}}(x,\omega)\mathbf{s}_R(x,\omega)\mathrm{d}x.\end{aligned} \tag{54}$$

Substituting Eq. (19) and Eq. (20) in Eq. (53) and Eq. (54), the random part of the stiffness and mass matrices as closed-form expressions can be obtained. Again, the closed-form expressions are found. Thus, only the matrix forms of $\mathbf{Sk}_L, \mathbf{Sk}_R, \mathbf{Sm}_L, \mathbf{Sm}_R$ for each jth terms, respecting the odd and even KL formulation, will be shown. By considering odd j, one has,

$$\mathbf{Sk}_L^{odd}(\omega) = \frac{EI_0}{\sqrt{\mathtt{a} + \frac{\sin(2w_j\mathtt{a})}{2w_j}}}\begin{bmatrix} SkLo_{11} & SkLo_{12} & SkLo_{13} & SkLo_{14}\\ & SkLo_{22} & SkLo_{23} & SkLo_{24}\\ & & SkLo_{33} & SkLo_{34}\\ Sym & & & SkLo_{44}\end{bmatrix},$$

$$\mathbf{Sk}_R^{odd}(\omega) = \frac{EI_0}{\sqrt{\mathtt{a} + \frac{\sin(2w_j\mathtt{a})}{2w_j}}}\begin{bmatrix} SkRo_{11} & SkRo_{12} & SkRo_{13} & SkRo_{14}\\ & SkRo_{22} & SkRo_{23} & SkRo_{24}\\ & & SkRo_{33} & SkRo_{34}\\ Sym & & & SkRo_{44}\end{bmatrix},$$

$$\mathbf{Sm}_L^{odd}(\omega) = \frac{\rho A_0}{\sqrt{\mathtt{a} + \frac{\sin(2w_j\mathtt{a})}{2w_j}}}\begin{bmatrix} SmLo_{11} & SmLo_{12} & SmLo_{13} & SmLo_{14}\\ & SmLo_{22} & SmLo_{23} & SmLo_{24}\\ & & SmLo_{33} & SmLo_{34}\\ Sym & & & SmLo_{44}\end{bmatrix},$$

$$\mathbf{Sm}_R^{odd}(\omega) = \frac{\rho A_0}{\sqrt{\mathtt{a} + \frac{\sin(2w_j\mathtt{a})}{2w_j}}}\begin{bmatrix} SmRo_{11} & SmRo_{12} & SmRo_{13} & SmRo_{14}\\ & SmRo_{22} & SmRo_{23} & SmRo_{24}\\ & & SmRo_{33} & SmRo_{34}\\ Sym & & & SmRo_{44}\end{bmatrix},$$

and for even j,

$$\mathbf{Sk}_L^{even}(\omega) = \frac{EI_0}{\sqrt{\mathtt{a} - \frac{\sin(2w_j\mathtt{a})}{2w_j}}}\begin{bmatrix} SkLe_{11} & SkLe_{12} & SkLe_{13} & SkLe_{14}\\ & SkLe_{22} & SkLe_{23} & SkLe_{24}\\ & & SkLe_{33} & SkLe_{34}\\ Sym & & & SkLe_{44}\end{bmatrix},$$

$$\mathbf{Sk}_R^{even}(\omega) = \frac{EI_0}{\sqrt{\mathtt{a} - \frac{\sin(2w_j\mathtt{a})}{2w_j}}}\begin{bmatrix} SkRe_{11} & SkRe_{12} & SkRe_{13} & SkRe_{14}\\ & SkRe_{22} & SkRe_{23} & SkRe_{24}\\ & & SkRe_{33} & SkRe_{34}\\ Sym & & & SkRe_{44}\end{bmatrix},$$

$$\mathbf{Sm}_L^{even}(\omega) = \frac{\rho A_0}{\sqrt{\mathtt{a} - \frac{\sin(2w_j\mathtt{a})}{2w_j}}}\begin{bmatrix} SmLe_{11} & SmLe_{12} & SmLe_{13} & SmLe_{14}\\ & SmLe_{22} & SmLe_{23} & SmLe_{24}\\ & & SmLe_{33} & SmLe_{34}\\ Sym & & & SmLe_{44}\end{bmatrix},$$

$$\mathbf{Sm}_R^{even}(\omega) = \frac{\rho A_0}{\sqrt{\mathtt{a} - \frac{\sin(2w_j\mathtt{a})}{2w_j}}}\begin{bmatrix} SmRe_{11} & SmRe_{12} & SmRe_{13} & SmRe_{14}\\ & SmRe_{22} & SmRe_{23} & SmRe_{24}\\ & & SmRe_{33} & SmRe_{34}\\ Sym & & & SmRe_{44}\end{bmatrix},$$

Considering that all parameters and matrices of Eqs. (51) and (52) are presented, it is easy to implement them in software similar to MATHEMATICA to obtain the random damage stiffness and mass matrices, $\mathbf{K}_j(\omega)$ and $\mathbf{M}_j(\omega)$. The stochastic spectral damaged beam dynamic stiffness matrix is obtained as

$$\mathbf{D}(\omega,\theta) = \mathbf{K}(\omega,\theta) - \omega^2\mathbf{M}(\omega,\theta). \tag{55}$$

4 Numerical simulation

By demonstrating the random field transformation via the memoryless transformation, the analysis provides a case where the target PDF is the Gamma distribution. Figure 3 shows the Gamma translation process expressed as a transformation of a homogeneous Gaussian field with zero mean, unit variance and exponential covariance function. The

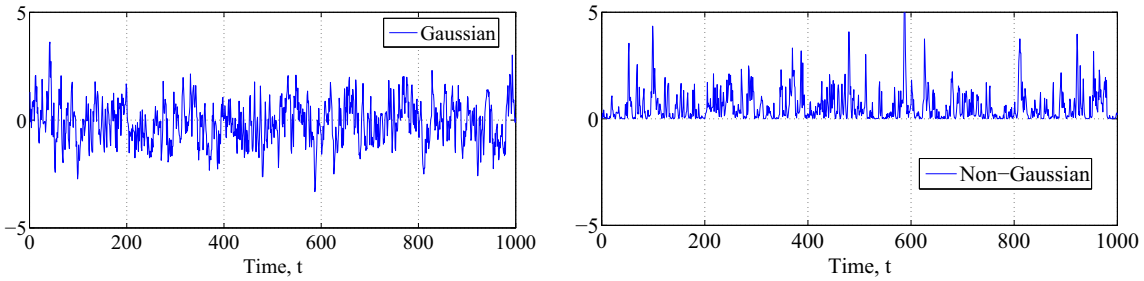

Fig. 3 Gaussian translation process with target (Gamma) distribution using third-order numerical approaches in a Hermite polynomial

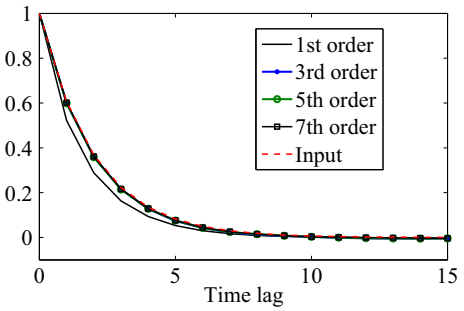

Fig. 4 Input covariance function compared with approximated covariance function estimated with 1–7 orders in a Hermite polynomial

projection of this transformation is based on the Hermite polynomial degree function (Eq. 28). The approximation of $Y(x,\theta)$, as a function of $Z(x,\theta)$, improves as the Hermite polynomial degree increases. Figure 4 shows the correlation function convergence related to the P-th order Hermite polynomial approximation, herein $P = 1, 3, 5$ and 7. The transformation with 3rd–7th order shows good agreement with the input correlation. It was performed for 10,000 realisations of the underlying Gaussian process, $Z(x,\theta)$.

Figure 5 illustrates the marginal PDF, $p_Y(y)$, of the zero mean non-Gaussian process obtained via transformation of the underlying Gaussian process. The first-order approximation of the transformation leads to a Gaussian process. The higher the polynomial degree, the better the convergence with the targeted PDF. The fifth-order approximation leads to a process with an acceptable, but marginal, PDF, whereas, with the seventh-order approximation, the curves are practically coincident.

Next, the analysed problem is a dynamic system modelled by using a Gaussian random field and a non-Gaussian random field target with a Gamma distribution, as demonstrated. This numerical example presents a free–free rod structure modelled by a two-node cracked-rod spectral element [39] with variabilities considered in the longitudinal rigidity, EA, and the mass per unit length, ρA. The measured frequency response function (FRF) simulates the receptance FRF with force excitation at node 1 and

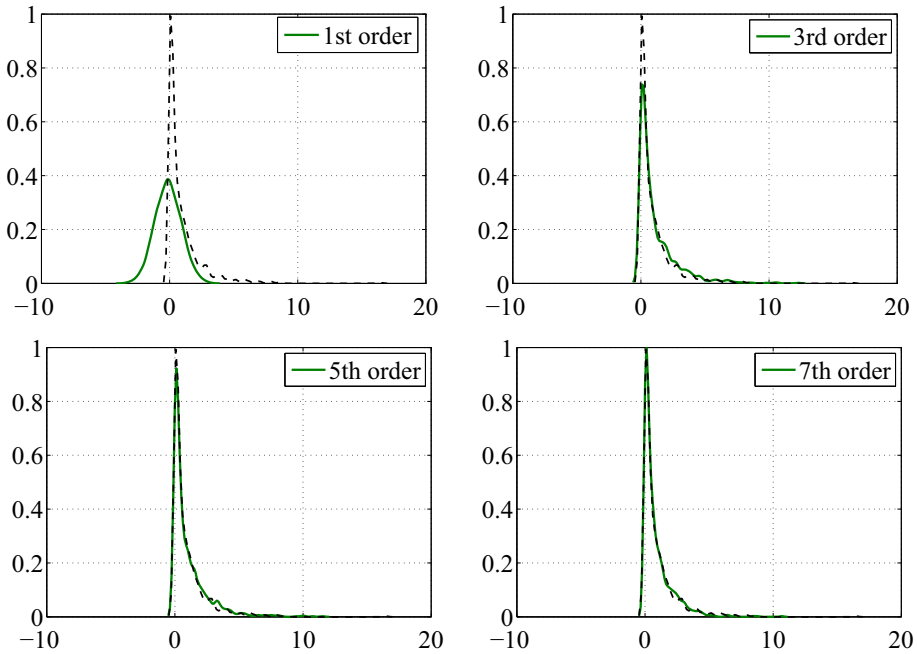

Fig. 5 Approximation of the $Y(t)$ PDF obtained through the Hermite polynomial expansion with P ranging from 1 to 7. In all tests, the number of samples is equal to 10,000

response at node 2. The unperturbed physical and geometrical properties of the rod are the length, $L = 0.35$ m, cross section height, $h = 0.02$ m, base, $b = 0.02$ m, crack position, $L_1 = 0.3L$ m, crack depth $\alpha = 10\%$ of the cross section height and damping factor $\eta = 0.01$. The material is polyamide with $\rho = 1250$ kg/m^3 and $E = 1.1$ GPa. The variations of unperturbed value, EA and ρA, are modelled by a homogeneous Gaussian random field and then transposed to a Gamma distribution using a memoryless transformation. For numerical calculations, it is considered 1, 5 and 10% for the coefficient of variation (COV) with a correlation length of $\mathrm{b} = L/3$ and four modes of KL expansion. The correlation length value is a chosen referent with the number of terms, as mentioned in [52].

The response is calculated up to 10,000 Hz, covering the 5-to-6 vibration modes of the system. Receptance FRF for the mean value, standard deviation of the absolute value and deterministic response of the rod for different COV's are shown in Figs. 6, 7 and 8. For all cases, the receptance curves of mean value and deterministic are very close. At lower frequencies, the standard deviation is biased by the mean. As the frequency increases, the standard deviation curve flattens. This behaviour is more accentuated with the increase in the COV. These results are obtained using a Monte Carlo simulation with 200 samples. The mean converges faster for small COVs. For all cases, approximately 120 realisations are necessary for the standard deviation square convergences.

The central goal of this paper is developing a stochastic spectral crack element. Whereas damage detection is not addressed, an example related to changes in the FRF owing to the crack depth variation is demonstrated. Consider the previous example, where the COV is 5%, and the crack depth is varied as $\alpha = \{0, 1, 10, 20, 30\}\%$ of cross section height. The receptance FRFs of mean and standard deviation for different crack depths are shown in Fig. 9. The mean receptance FRF without crack ($\alpha = 0$), compared to the FRFs with crack depths of $\alpha = 1\%$ and 10%, presents no significant changes in the frequency range of 0–5 kHz. However, for crack depths of $\alpha = 20\%$ and 30%, the frequency shifts and amplitude variations are present in almost all resonance peaks of the analysed band. By associating the mean FRFs with the standard deviation envelope of FRFs considering COV of 5%, they are small at low frequencies and small crack depths (1 and 10%), but become larger as the frequency increases up to 5 kHz and crack depths grow (20 and 30%). The standard deviation curve flattening behaviour is more accentuated at frequencies higher than 5 kHz and larger crack depths. The changes in dynamic response can be related to changes in geometry and structural material properties. The use of a stochastic model is one way to address the randomness of the structure in damage detection problems.

Another example, consisting of a free–free beam structure modelled by a two-node beam spectral element, is considered. Variabilities of the beam flexural rigidity, EI,

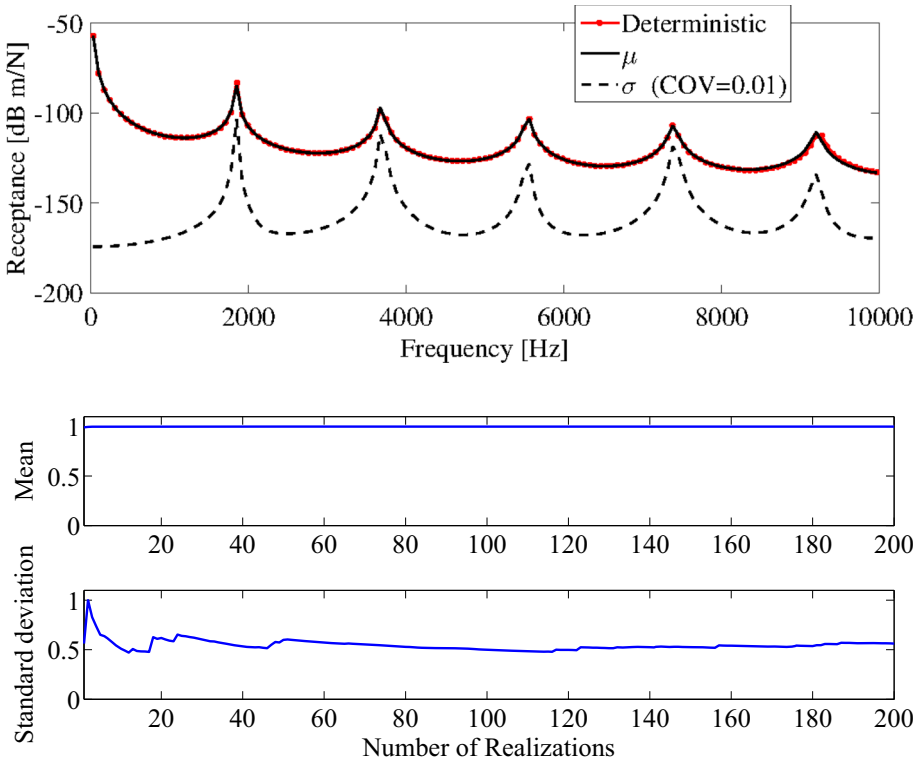

Fig. 6 Rod deterministic, mean (μ), standard deviation (σ) FRF and convergence analyse for COV of 1%

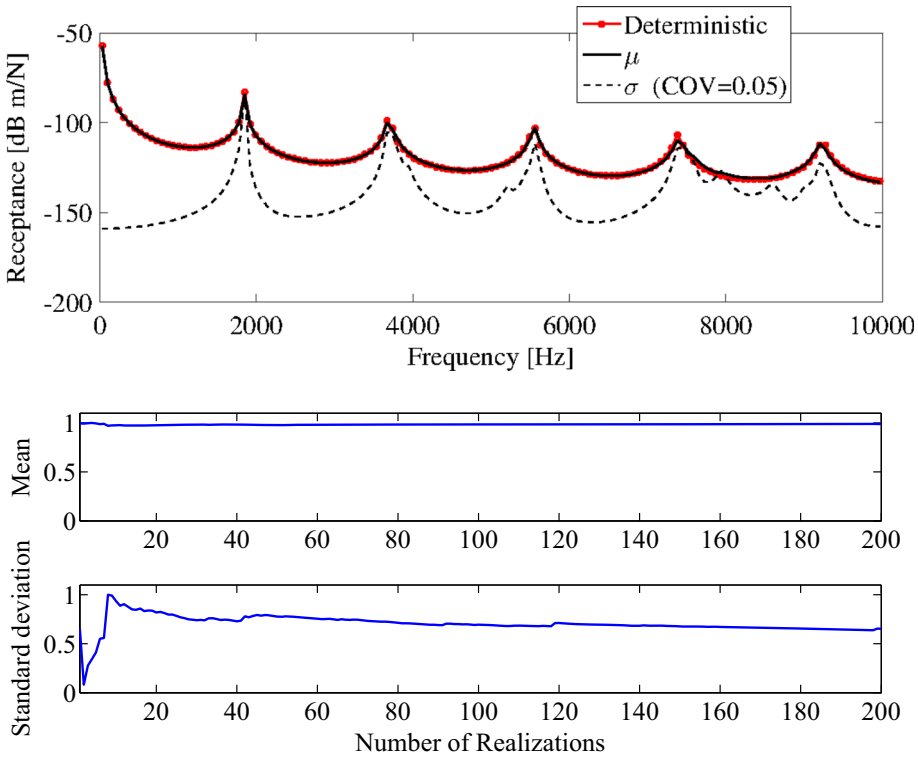

Fig. 7 Rod deterministic, mean (μ), standard deviation (σ) FRF and convergence analysis for COV of 5%

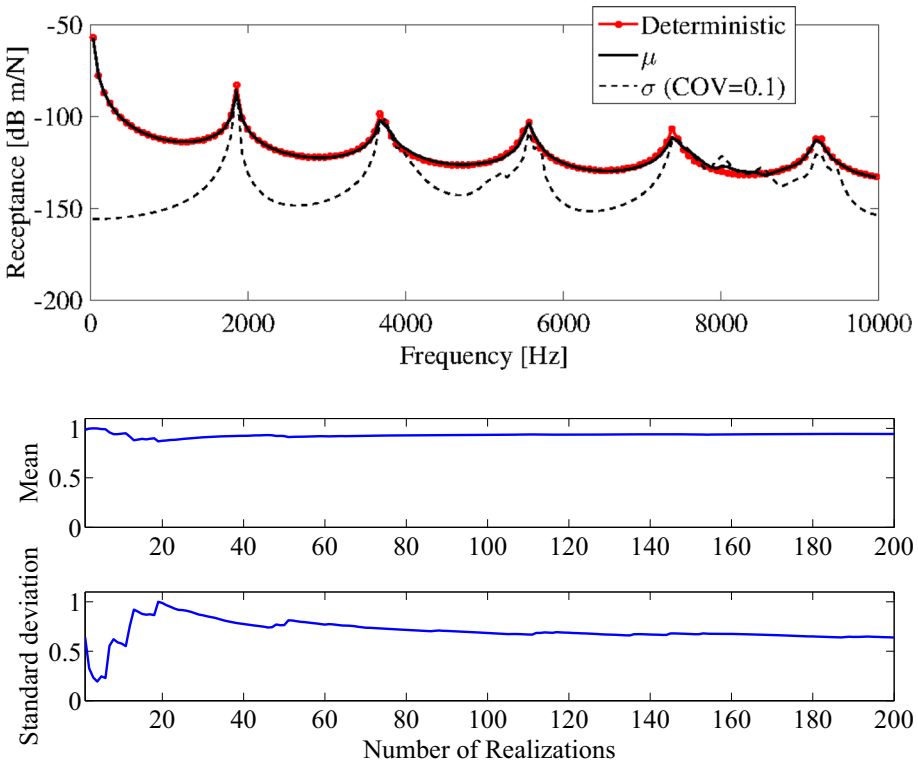

Fig. 8 Rod deterministic, mean (μ), standard deviation (σ) FRF, and convergence analysis for COV of 10%

and mass per unit length, ρA are considered and both structural variabilities are Gamma marginal distributions. The measured FRF simulates the transfer receptance FRF with force excitation at node 1 and displacement response at node 2. The geometric parameters of the beam are length, $L = 0.35$ m, cross section, $h = 0.006 \times b = 0.018$ m, crack position, $L_1 = 0.3L$ m, crack depth $\alpha = 10\%$ of cross section height and damping factor, $\eta = 0.01$. The

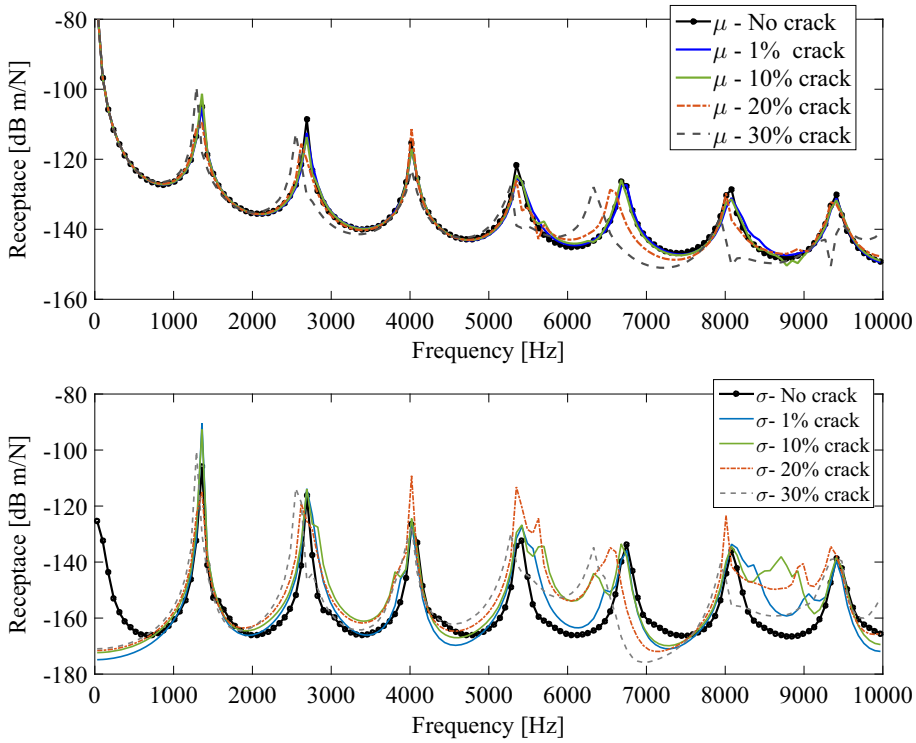

Fig. 9 FRF mean and standard deviation amplitudes for a cracked rod with various crack depth ratios (uncracked, $\alpha = 1\%$, $\alpha = 10\%$, $\alpha = 20\%$ and $\alpha = 30\%$). The coefficient of variation is 5% for all cases

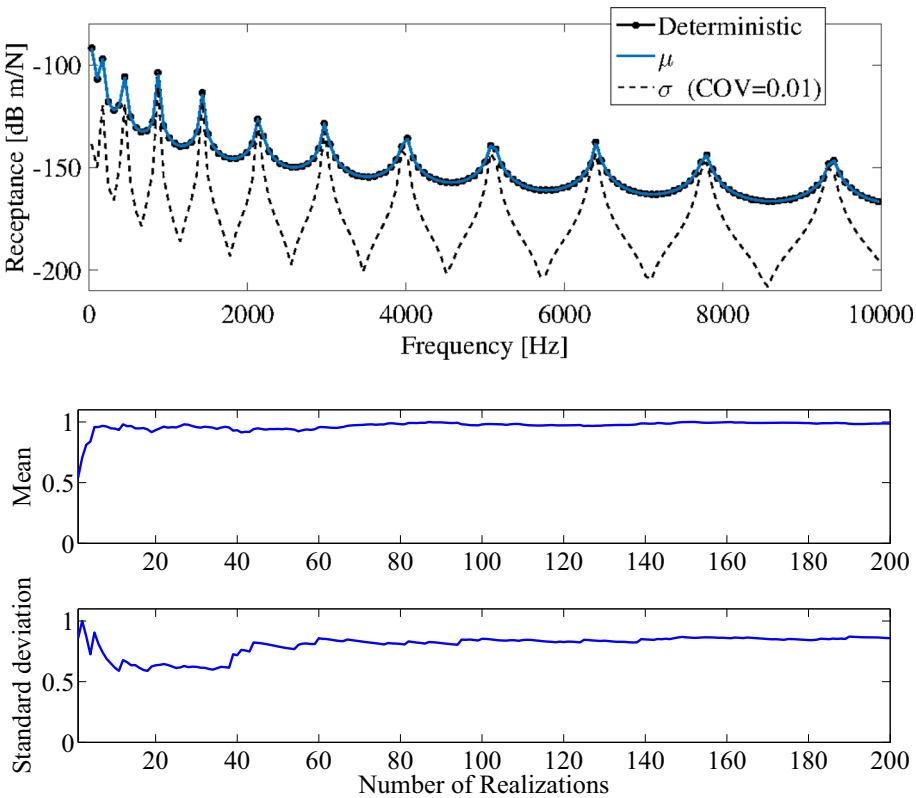

Fig. 10 Beam deterministic, mean (μ), standard deviation (σ) FRF and convergence analysis for COV of 1%

material properties and random fields are the same as in the previous examples.

The receptance FRFs of deterministic, mean and standard deviation, calculated up to 10 kHz for COVs = 1, 5 and 10%, are shown in Figs. 10, 11 and 12, respectively. These results are obtained using a Monte Carlo simulation with 200 samples, presenting a convergence test calculated using Eq. 29. For all cases, the mean FRF is very close to

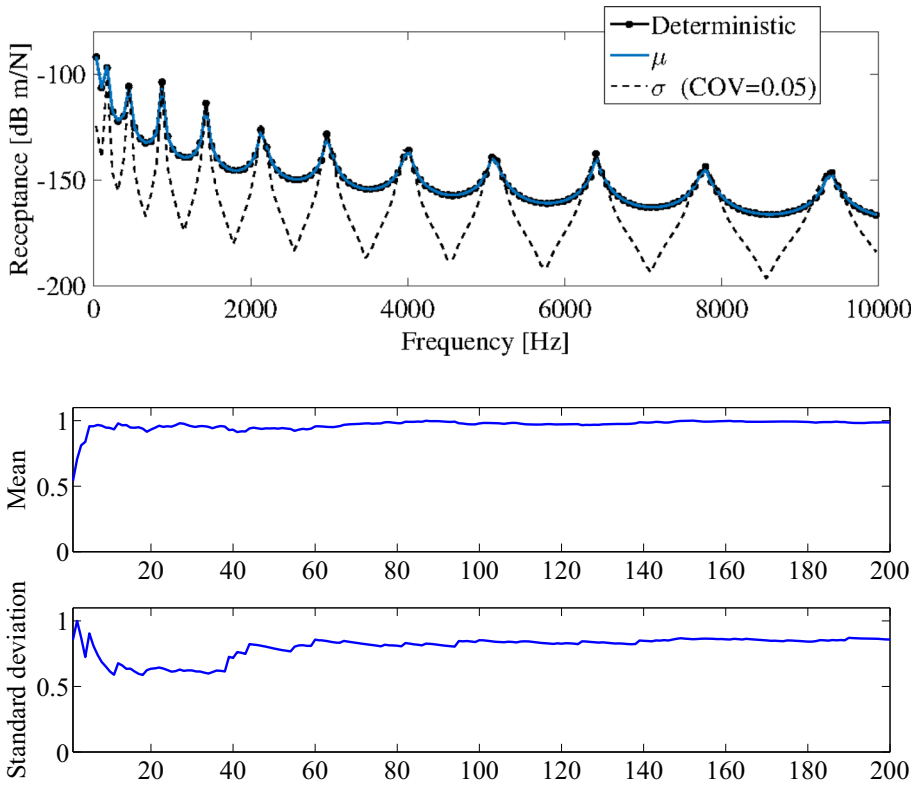

Fig. 11 Beam deterministic, mean (μ), standard deviation (σ) FRF and convergence analysis for COV of 5%

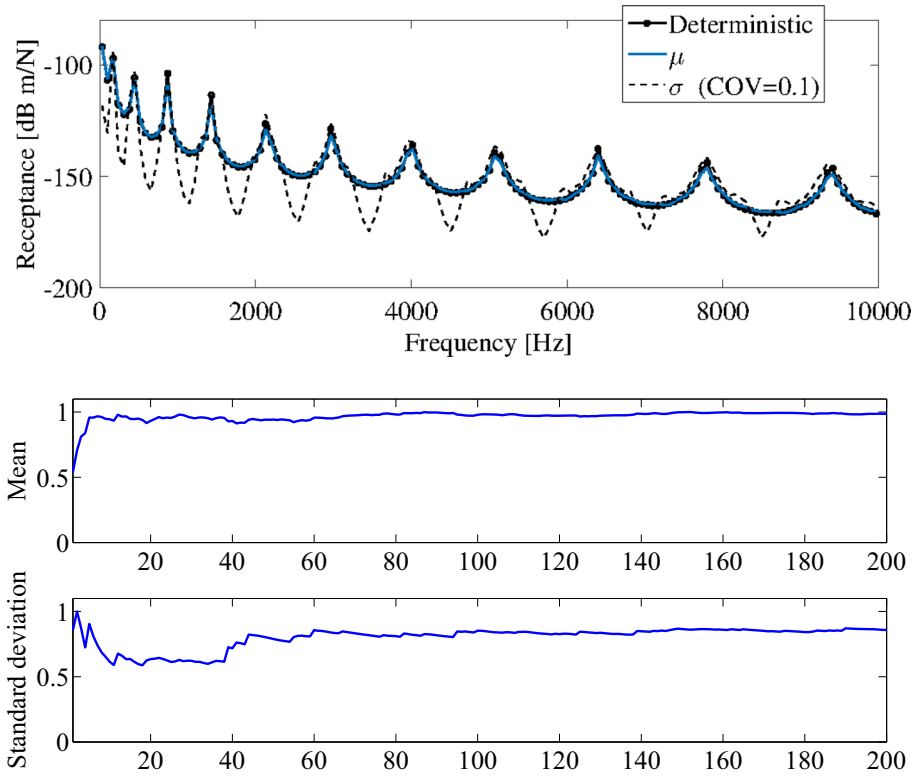

Fig. 12 Beam deterministic, mean (μ), standard deviation (σ) FRF and convergence analysis for COV of 10%

the deterministic FRF, and the standard deviation is biased by the mean. However, at higher frequencies, the standard deviation FRF flattens, which could be influenced by the damping of our stochastic approach. The square convergence of the mean and standard deviation is calculated for 200 realisations, converging near 150.

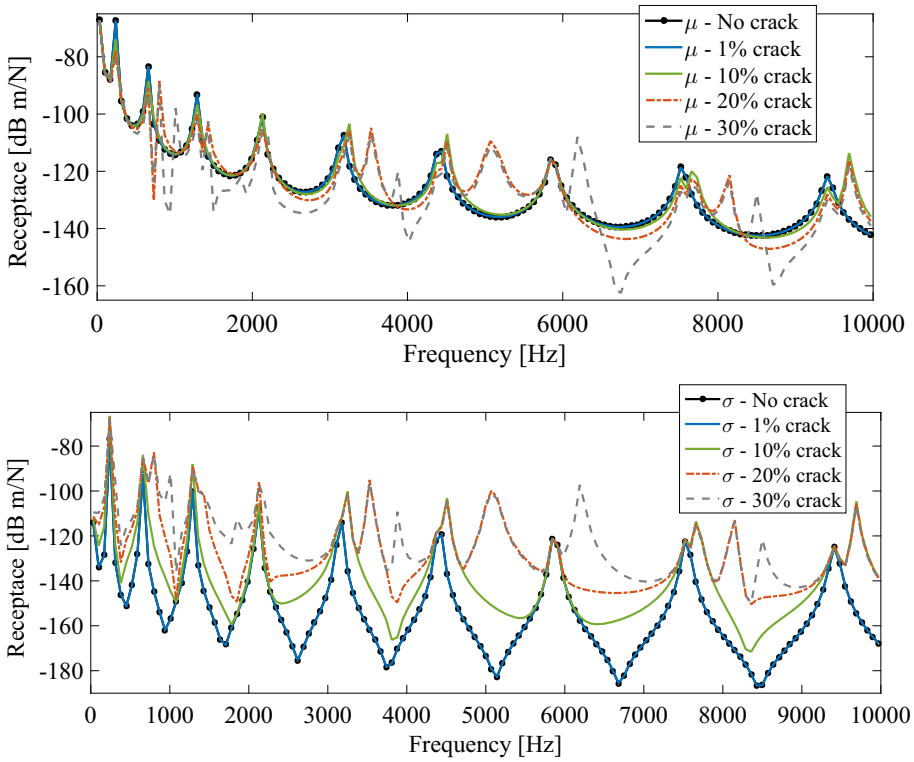

Fig. 13 FRF mean and standard deviation amplitudes for a cracked beam with various crack depth ratios (uncracked, $\alpha = 1\%$, $\alpha = 10\%$, $\alpha = 20\%$ and $\alpha = 30\%$). The coefficient of variation is 5% for all cases

Likewise, for the rod structure, an analysis related to changes in the FRF, caused by the crack depth variation, is also performed for the beam. By using the same cracked beam properties and parameters, COV is 5% and the crack depth variation is $\alpha = \{0, 1, 10, 20, 30\}\%$ of cross section height. Figure 13 shows the mean and standard deviation receptance FRFs of the cracked beam with different crack depths. In this case, at low-frequency ranges, the mean FRF without crack, compared to cracked beam responses for small crack depths, do not exhibit significant changes. However, as the frequency increases (up to 800 Hz) and for crack depths from 20 to 30%, a considerable change in FRFs, related to shifts in the resonance frequency and changes in amplitude, are observed. The standard deviation FRF flattens. This behaviour is more accentuated at higher frequency bands with larger crack depths. By associating the mean responses with the standard deviation envelope for crack depths greater than 10%, we notice a whole frequency range. As the crack depth increases, the standard deviation response envelope exhibits similar behaviour.

5 Conclusion

The formulation of a 1D damaged structure with distributed parametric uncertainty was proposed. The spatial displacement fields were discretised using frequency-complex shape functions. The spatial random fields were discretised using the KL expansion. This paper unified the two techniques aiming to use SEM to model damaged structure elements, considering distributed uncertainties in the parameters. The resulting frequency-dependent random element matrices, in general, turned out to be complex symmetric matrices. The detailed derivations for a damaged beam in bending vibration were given. Numerical examples demonstrated the applicability of the proposed method, which was solved using a Monte Carlo simulation. Thus, a convergence technique should be applied to verify the suitability of the number of samples. The presented methodology was compared to the deterministic approach presented in the literature; good agreement was observed and efficiency noted. The use of a stochastic model is a way to predict randomness in the structure in damage detection problems.

References

1. Zienkiewicz OC, Taylor RL (2000) The finite element method. Butterworth-Heinemann, Oxford
2. Ghanem R, Spanos P (1991) Stochastic finite elements: a spectral approach. Springer, New York
3. Ghanem R, Kruger RM (1996) Numerical solution of a spectral stochastic finite element systems. Comput Methods Appl Mech Eng 129:289–303

4. Stefanou G (2009) The stochastic finite element method: past, present and future. Comput Methods Appl Mech Eng 198:1031–1051
5. Banerjee JR (1997) Dynamic stiffness formulation for structural elements a general approach. Comput Struct 63(1):101–103
6. Lee U (2004) Spectral element method in structural dynamics. Inha University Press, Incheon
7. Doyle JF (1997) Wave propagation in structures: spectral analysis using fast discrete Fourier transforms. Mechanical engineering, 2nd edn. Springer, New York
8. Beskos D, Narayanan G (1978) Use of dynamic influence coefficients in forced vibration problems with the aid of fast fourier transform. Comput Struct 9(2):145–150
9. Spyrakso C, Beskos D (1982) Dynamic response of frameworks by fast fourier transform. Comput Struct 15(5):495–505
10. Doyle JF (1989) Wave propagation in structures. Springer, New York
11. Paz M (1980) Structural dynamics: theory and computation, 2nd edn. Van Nostrand, Reinhold
12. Banerjee JR, Williams FW (1985) Exact Bernoulli–Euler dynamic stiffness matrix for a range of tapered beams. Int J Numer Methods Eng 21(12):2289–2302
13. Banerjee JR (1989) Coupled bending torsional dynamic stiffness matrix for beam elements. Int J Numer Methods En 28(6):1283–1298
14. Banerjee JR, Williams FW (1992) Coupled bending-torsional dynamic stiffness matrix for Timoshenko beam elements. Comput Struct 42(3):301–310
15. Banerjee JR, Fisher SA (1992) Coupled bending torsional dynamic stiffness matrix for axially loaded beam elements. Int J Numer Methods Eng 33(4):739–751
16. Ferguson NJ, Pilkey WD (1993) Literature review of variants of dynamic stiffness method. Part 1: the dynamic element method. Shock Vib Dig 25(2):3–12
17. Ferguson NJ, Pilkey WD (1993) Literature review of variants of dynamic stiffness method. Part 2: frequency-dependent matrix and other. Shock Vib Dig 25(4):3–10
18. Banerjee JR, Williams FW (1995) Free-vibration of composite beams: an exact method using symbolic computation. J Aircr 32(3):636–642
19. Manohar CS, Adhikari S (1998) Dynamic stiffness of randomly parametered beams. Probab Eng Mech 13(1):39–51
20. Banerjee JR (1997) Dynamic stiffness formulation for structural elements: a general approach. Comput Struct 63(1):101–103
21. Adhikari S, Manohar CS (2000) Transient dynamics of stochastically parametered beams. ASCE J Eng Mech 126(11):1131–1140
22. Finnveden S (1997) Spectral finite element analysis of the vibration of straight fluid filled pipes with flanges. J Sound Vib 199(1):125–154. https://doi.org/10.1006/jsvi.1996.0602
23. Gopalakrishnan S, Chakraborty A, Mahapatra DR (2007) Spectral finite element method. Springer, New York
24. Hashemi SM, Richard MJ, Dhatt G (1999) A new dynamic finite element (DFE) formulation for lateral free vibrations of Euler–Bernoulli spinning beams using trigonometric shape functions. J Sound Vib 220(4):601–624
25. Hashemi SM, Richard MJ (2000) Free vibrational analysis of axially loaded bending-torsion coupled beams: a dynamic finite element. Comput Struct 77(6):711–724
26. Doyle JF (1988) A spectrally formulated finite elements for longitudinal wave propagation. J Anal Exp Modal Anal 3:1–5
27. Ostachowicz W, Kudela P, Krawczuk M, Zak A (2012) Guided waves in structures for SHM. Wiley, London. https://doi.org/10.1002/9781119965855
28. Ajith V, Gopalakrishnan S (2010) Spectral element approach to wave propagation in uncertain beam structures. J Mech Mater Struct 5(4):637–659
29. Adhikari S (2011) Doubly spectral stochastic finite-element method for linear structural dynamics. Am Soc Civ Eng 1:264–276
30. Doebling SW, Farrar CR, Prime M (1998) A review of vibration-based damage identification methods. Technical report, Engineering Analysis Group Los Alamos National Laboratory
31. Montalvao D, Maia N, Ribeiro A (2006) A review of vibration-based structural health monitoring with special emphasis on composite materials. Shock Vib Dig 38:10–22
32. Krawczuk M (2002) Application of spectral beam finite element with a crack and iterative search technique for damage detection. Finite Elem Anal Des 80:1809–1816. https://doi.org/10.1016/S0168-874X(01)00084-1
33. Krawczuk M, Grabowska J, Palacz M (2006) Longitudinal wave propagation. Part I: comparison of rod theories. J Sound Vib 295:461–478. https://doi.org/10.1016/j.jsv.2005.12.048
34. Ostachowicz WM (2008) Damage detection of structures using spectral finite element method. Comput Struct 86:454–462. https://doi.org/10.1016/j.compstruc.2007.02.004
35. Santos E, Arruda J, Santos JD (2008) Modeling of coupled structural systems by an energy spectral element method. J Sound Vib 36:1–24
36. Su Z, Ye L (2009) Identification of damage using lamb waves. Springer, New York
37. Fabro AT, Ritto TG, Sampaio R, Arruda JRF (2010) Stochastic analysis of a cracked rod modeled via the spectral element method. Mech Res Commun 37:326–331. https://doi.org/10.1016/j.mechrescom.2010.03.005
38. Ng C, Veidt M, Lam H (2011) Probabilistic damage characterisation in beams using guided waves. Procedia Eng 14:490–497
39. Machado M, Adhikari S, Santos J (2017) A spectral approach for damage quantification in stochastic dynamic systems. Mech Syst Signal Process 88:253–273. https://doi.org/10.1016/j.ymssp.2016.11.018
40. Flynn EB, Todd M, Croxford J, Drinkwater B, Wilcox P (2012) Enhanced detection through low-order stochastic modeling for guided-wave structural health monitoring. Struct Health Monit 1:1–12. https://doi.org/10.1177/1475921711414232
41. Machado MR, Santos JMCD (2015) Reliability analysis of damaged beam spectral element with parameter uncertainties. Shock Vib. https://doi.org/10.1155/2015/574846
42. Schevenels GLM, Degrande G (2004) Application of the stochastic finite element method for Gaussian and non-Gaussian systems. In: Proceedings of international conference on noise and vibration engineering
43. Meirovitch L (1997) Principles and techniques of vibrations. Prentice-Hall, Upper Saddle River
44. Papoulis A, Pillai SU (2002) Probability, random variables and stochastic processes, 4th edn. McGraw-Hill, Boston
45. Vio R, Andreani P, Wamsteker W (2001) Numerical simulation of non-Gaussian random fields with prescribed correlation structure. Technical report, ESA IUE Obsevatory and Max-Planck Institut fur Extraterrestrische Physik
46. Phoon KK, Huang HW, Quek ST (2005) Simulation of strongly non-Gaussian processes using Karhunen–Loeve expansion. Struct Saf 20(2):188–198. https://doi.org/10.1016/j.probengmech.2005.05.007
47. Shields M, Deodatis G, Bocchinic P (2011) A simple and efficient methodology to approximate a general non-Gaussian stationary stochastic process by a translation process. Probab Eng Mech 26:511–519

48. Grigoriu M (1998) Simulation of stationary non-Gaussian translation processes. J Eng Mech 124(2):121–126. https://doi.org/10.1061/(ASCE)0733-9399(1998)124:2(121)
49. Weinberg G, Gunn L (2011) Simulation of statistical distributions using the memoryless nonlinear transformation. Technical report, DSTO Defence Science and Technology Organisation-Australia Government
50. Rubinstein R, Kroese D (2008) Simulation and the Monte Carlo method. Wiley, New York
51. Krawczuk M, Palacz M, Ostachowicz W (2002) The dynamic analysis of a cracked Timoshenko beam by the spectral element method. J Sound Vib 264:1139–1153. https://doi.org/10.1016/S0022-460X(02)01987-1
52. Xiu D (2010) Numerical methods for computations: a spectral method approach. Princeton University Press, Princeton